Semiclassical theory of multisubband plasmons: Nonlocal electrodynamics and radiative effects

Filippo Alpeggiani[*] and Lucio Claudio Andreani
Dipartimento di Fisica, Università degli Studi di Pavia and CNISM, Via Bassi 6, 27100 Pavia, Italy
(Received 16 June 2014; revised manuscript received 28 July 2014; published 25 September 2014)

Coherent multisubband plasmons in doped semiconductor quantum wells have recently attracted large interest as they allow us to strongly enhance light-matter interaction via collective Coulomb coupling among different intersubband transitions. In this work, we develop a semiclassical theory of intersubband plasmons in quantum wells, on the basis of nonlocal electrodynamics. The nonlocal treatment provides a proper description of collective effects in the electromagnetic response of the system and, in the long-wavelength approximation, it predicts the same resonance frequencies as the quantum mechanical description. The nonlocal formalism is applied to the study of the radiative decay rate of multisubband plasmons and plasmon polaritons, both in the case of an isolated quantum well and of a planar microcavity. We show that subpicosecond radiative lifetimes are to be expected for intersubband plasmons in semiconductor quantum wells, similarly to quantum well excitons. The theory is formulated in the context of the transfer-matrix method and it can be applied in a straightforward way to stratified geometries of any degree of complexity.

I. INTRODUCTION

It is well known that the intersubband electromagnetic response of a semiconductor quantum well (QW) is a collective phenomenon [1–5]. Major evidence for this collective behavior is a shift in the absorption frequency of intersubband transitions with respect to the energy-level separation, whose main contribution, the so-called depolarization shift, can be thought as a dynamical (time-dependent) Hartree correction of the resonance frequency. A second contribution with opposite sign originating from the dynamical exchange-correlation term, the so-called final-state interaction or exciton correction [3,6], for QWs is generally of far lesser extent [7,8] and it is not considered in this work. For a two-level system, the presence of the depolarization shift is already accounted for by a simple slab model for the two-dimensional electron gas [2]; the same results can also be obtained with a nonlocal electrodynamic treatment [4,5]. Some generalizations to multilevel systems have been derived [1,9–11]. The collective response of the QW can be understood in terms of the coupling between photons and a family of excitations represented by intersubband transitions dressed by the mutual electrostatic interaction, called intersubband plasmons (IPs) [12,13]. In addition to optical absorption experiments, intersubband plasmons have also been studied by other techniques, such as inelastic light scattering [14,15].

Recently, interest on the intersubband response of two-dimensional systems has been renewed by the demonstration that, in a QW with several occupied subbands, the very same cooperative mechanism that is responsible for the depolarization shift induces a redistribution of the spectral weight of intersubband transitions, which eventually concentrates on a single sharp resonance, to be associated with the so-called bright multisubband plasmon [16,17]. This represents a very promising approach for attaining infrared superradiant emission or for studying the ultrastrong-coupling regime of light-matter interaction [13,18]. Moreover, the effect is naturally

suited to be controlled by tailoring the two-dimensional charge density in the QW, e.g., by the use of a gate potential [19]. It is clear that, in view of further development in the field, a deeper knowledge of the radiative dynamics of multisubband plasmons, including, for instance, the behavior of radiative lifetime and the effect of incoherent scattering channels, would turn extremely beneficial.

A quantum mechanical theory of the intersubband response of a QW has been recently developed [13]. The theory is based on the electrical dipole gauge and it shows that both the depolarization and multisubband plasmon effects originate from the quadratic polarization term P^2 of the dipolar Hamiltonian. A new family of operators, which are to be associated to intersubband plasmons, are constructed from a Hopfield-Bogoljubov transformation of the bare intersubband operators in the presence of reciprocal coupling induced by the P^2 term. The quantum formulation is an essential benchmark in the theoretical treatment of multisubband plasmons, yet it is not easily turned into a calculation of the optical properties.

Despite different characteristic frequencies, optical properties of intersubband plasmons have strong analogies with those of Z-polarized excitons in QWs, which have been extensively studied in the previous years [20–22]. The analogy is related to the fact that both excitations can be modeled semiclassically as planes of oscillating dipoles polarized along the growth axis of the QW. The radiative lifetime of two-dimensional excitons [23–27] is expected to have a counterpart for intersubband plasmons. In addition, the study of microcavity exciton-polaritons led to very exciting phenomena such as stimulated emission and even Bose-Einstein condensation [28,29]. However, an important difference with multisubband plasmons is that, whereas the optical response of QWs is generally characterized by the excitation of a single exciton mode, the collective intersubband response can be strongly affected by the mutual interaction of multiple intersubband transitions.

In this work, we present a semiclassical theory of the intersubband response of a generic QW based on nonlocal electrodynamics, following the lines of Ref. [10]. The framework is quite general and it is easily adapted to a variety

---

*filippo.alpeggiani01@ateneopv.it

of situations. In particular, we present our results by means of the transfer-matrix formalism [30–34], which proves itself extremely handy when dealing with layered systems. In the long-wavelength approximation, our semiclassical results for the frequencies of multisubband plasmons agree with those from quantum theory, as expected for systems with a quadratic Hamiltonian in the photon and polarization operators. In order to illustrate the application of the theory, we focus on the problem of the radiative decay rate of multisubband plasmons and perform a detailed analysis following both a perturbative and a nonperturbative approach. We also consider the presence of metallic mirrors in the vicinity of the QW, showing that the theory is also suitable for the analysis of intersubband plasmon polaritons in planar microcavities [13,35,36]. The nonlocal electrodynamics theory can be easily applied to layered structures of any degree of complexity.

The paper is organized as follows. In Sec. II, we present the semiclassical theory for the intersubband response of a QW based on nonlocal electrodynamics, first in the general case and, then, in the long-wavelength approximation. In the latter situation, our results are compared with those from quantum theory. In Sec. III, we apply our formalism to the study of the radiative decay rate of multisubband plasmons, including the effect of nonradiative decay channels. More elaborate systems characterized by the presence of metal-dielectric interfaces, such as planar optical cavities, are taken into account in Sec. IV. Finally, Sec. V contains concluding remarks, whereas Appendices A and B present two side derivations for comparison with the results in the main text.

II. NONLOCAL THEORY

A. General formalism

We consider a QW embedded in a slab of thickness L, defined as a characteristic length beyond which the subband wave functions of the QW are approximately null. The static dielectric constant of the medium is ε_s (for simplicity, we neglect the slight difference in the static dielectric constant of the well and barrier materials). The nonlocal susceptibility tensor of the QW can be calculated in the context of the effective mass and random-phase approximations (RPA) [12,37–39] where the nondiagonal components can be omitted. We suppose the z axis oriented along the growth direction. After applying the Fourier transform in the xy plane ($\boldsymbol{q}$ is the in-plane momentum difference), the z component of the nonlocal susceptibility tensor reads as

$$\chi_{zz}^{(\mathrm{RPA})}(\omega,\boldsymbol{q};z,z') = \sum_{\alpha} \chi_{\alpha}(\omega,\boldsymbol{q})\,\xi_{\alpha}(z)\,\xi_{\alpha}(z'), \quad (1)$$

where the notation $\alpha = (n,n')$ indicates the transition from subband n to subband n' and the current distribution $\xi_{\alpha}(z)$ is a function of the subband wave functions:

$$\xi_{\alpha}(z) = \psi_n(z)\,\partial_z \psi_{n'}(z) - \partial_z \psi_n(z)\,\psi_{n'}(z). \quad (2)$$

If the energy of the state with in-plane momentum $\boldsymbol{k}$ in subband n is $\hbar\omega_n(\boldsymbol{k}) = \hbar\omega_n^0 + \hbar^2 k^2/2m^*$, $f_{n\boldsymbol{k}}$ is the corresponding occupation number, and S the area of the QW, the single-
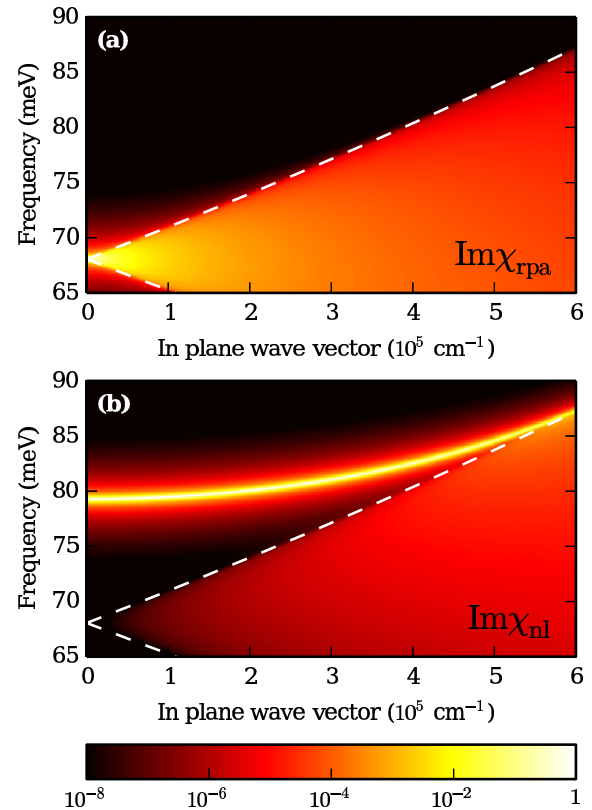

FIG. 1. (Color online) Single-particle and collective response of a 12-nm-thick $Al_{0.3}Ga_{0.7}As/GaAs$ quantum well uniformly doped with a density of $10^{12}\,cm^{-2}$ (only the first subband occupied; nonparabolicity effects neglected; static Hartree correction included): (a) Im $\chi_{12}(\omega,\boldsymbol{q})$, calculated from Eq. (3) for the $1 \rightarrow 2$ transition; (b) Im $\chi_{zz}^{(\mathrm{nl})}(\omega,\boldsymbol{q})$ according to Eq. (14). Both quantities are normalized to unity. Dashed white lines indicate the boundaries of the single-particle continuum.

particle susceptibility for the transition α is written [39]

$$\chi_{\alpha}(\omega,\boldsymbol{q}) = -\frac{1}{\omega^2}\frac{\hbar e^2}{\varepsilon_0 \omega_{\alpha} S (m^*)^2}\sum_{\boldsymbol{k}}(f_{n\boldsymbol{k}} - f_{n'\boldsymbol{k}+\boldsymbol{q}})$$

$$\times \left[1 + \frac{\omega_{\alpha}(\boldsymbol{k},\boldsymbol{q})\,\omega_{\alpha}}{(\omega + i\eta)^2 - \omega_{\alpha}^2(\boldsymbol{k},\boldsymbol{q})}\right];$$

$$\omega_{\alpha}(\boldsymbol{k},\boldsymbol{q}) = \omega_{n'}(\boldsymbol{k}+\boldsymbol{q}) - \omega_n(\boldsymbol{k});$$

$$\omega_{\alpha} = \omega_{n'}^0 - \omega_n^0. \tag{3}$$

For instance, in Fig. 1(a) we show Im $\chi_{12}(\omega,\boldsymbol{q})$ for the $1 \rightarrow 2$ transition of a QW with only the first subband occupied. In all the numerical results presented in this work, subband energies have been calculated at zero temperature including the static Hartree correction with a self-consistent method [40]. At $q=0$, the resonance is centered on the energy-level separation at 68 meV; with increasing q, the continuum of single-particle excitations is clearly recognizable. Equation (3) can be used also in the presence of nonparabolicity in the semiconductor conduction band [35,41], provided that the energies $\omega_n(\boldsymbol{k})$ and wave functions $\psi_n(z)$ are replaced with those obtained, e.g., from the effective-mass procedure of Ref. [42].

When dealing with layered systems, it is useful to solve electromagnetic problems by means of the transfer-matrix technique [30,31,33]. Intersubband transitions interact only with radiation with transverse magnetic (TM) polarization. We consider the case of a QW with inversion symmetry with respect to the $z = 0$ plane. Then, in the regions $z < -L/2$ and $z > L/2$, which we indicate with indices 1 and 2, respectively, the x component of the electric field can be written in the form of traveling waves ($k_z^2 = \varepsilon_s \omega^2/c^2 - q^2$)

$$E_{x,j}(z) = A_j e^{ik_z z} + B_j e^{-ik_z z} \quad (j = 1,2). \tag{4}$$

The transfer matrix of the QW, $\mathbb{T}_{\mathrm{QW}}$, is the 2×2 matrix that propagates the electric field across the QW

$$\begin{bmatrix} A_2 \\ B_2 \end{bmatrix} = \mathbb{T}_{\mathrm{QW}} \begin{bmatrix} A_1 \\ B_1 \end{bmatrix} \tag{5}$$

and can be calculated following a procedure analogous to that introduced in Ref. [21] for QW excitons.

Starting from the nonlocal RPA susceptibility in Eq. (1), from the application of Maxwell equations we obtain an integrodifferential equation for the z component D_z of the electric displacement field in the region $-L/2 < z < L/2$:

$$\left(\partial_z^2 + k_z^2 \right) D_z(z) = - \sum_\alpha \frac{\chi_\alpha(\omega, \boldsymbol{q})}{\varepsilon_s}$$
$$\times \, \xi_\alpha(z) \int dz' \, \xi_\alpha(z') \left(\partial_{z'}^2 + \frac{\omega^2}{c^2} \varepsilon_s \right) D_z(z'). \tag{6}$$

After setting

$$F_\alpha = \left[\int dz \, \xi_\alpha(z) \left(\partial_z^2 + \frac{\omega^2}{c^2} \varepsilon_s \right) D_z(z) \right] \bigg/ (q^2 \mathcal{A}), \tag{7}$$

we can write a solution of Eq. (6) in the form

$$D_z(z) = \mathcal{A} \left[\cos(k_z z) + q^2 \sum_\alpha \frac{\chi_\alpha(\omega, \boldsymbol{q})}{\varepsilon_s} F_\alpha \right.$$
$$\left. \times \int dz' \, \xi_\alpha(z') g(z,z') \right] + \mathcal{B} \sin(k_z z), \tag{8}$$

with the Green's function $g(z,z') = -\sin(k_z|z - z'|)/2k_z$ and $\mathcal{A}, \mathcal{B}$ being arbitrary constants.

By self-replacing Eq. (8) into Eq. (7), the following linear problem for the coefficients F_α is obtained:

$$F_\alpha + \sum_{\alpha'} F_{\alpha'} \left\{ \frac{\chi_{\alpha'}(\omega, \boldsymbol{q})}{\varepsilon_s} [I_{\alpha,\alpha'} + q^2 D_{\alpha,\alpha'}(k_z)] \right\}$$
$$= \int dz \, \cos(k_z z) \xi_\alpha(z), \tag{9}$$

where

$$I_{\alpha,\alpha'} = \int dz \, \xi_\alpha(z) \xi_{\alpha'}(z), \tag{10}$$

$$D_{\alpha,\alpha'}(k_z) = \frac{1}{2k_z} \int dz \, dz' \, \xi_\alpha(z) \sin(k_z|z - z'|) \xi_{\alpha'}(z'). \tag{11}$$

Once the coefficients F_α are calculated, the transfer matrix for the QW is readily worked out by imposing the boundary conditions at $z = \pm L/2$ for D_z, E_x, and their respective derivatives. The resulting transfer matrix is

$$\mathbb{T}_{\mathrm{QW}} = \begin{bmatrix} (1 + iC)e^{ik_z L} & -iC \\ iC & (1 - iC)e^{-ik_z L} \end{bmatrix}, \tag{12}$$

with

$$C = q^2 \chi_{zz}^{(\mathrm{nl})}(\omega, \boldsymbol{q})/(2k_z) \tag{13}$$

and the nonlocal susceptibility[1]

$$\chi_{zz}^{(\mathrm{nl})}(\omega, \boldsymbol{q}) = \sum_\alpha \frac{\chi_\alpha(\omega, \boldsymbol{q})}{\varepsilon_s} F_\alpha \int dz \, \cos(k_z z) \xi_\alpha(z). \tag{14}$$

As an example, Fig. 1(b) shows Im $\chi_{zz}^{(\mathrm{nl})}(\omega, \boldsymbol{q})$ for the system whose single-particle response is represented in Fig. 1(a). This simple example already reveals some typical features of the collective response of QW electrons: (i) the presence of a depolarization shift in the absorption frequency, which, in the $q = 0$ case, shifts the intersubband resonance from 68 to 79 meV [1–3]; (ii) the finite and narrow linewidth of the collective absorption peak in contrast with the broadening of the single-particle continuum [43,44]; (iii) the onset of Landau damping when the collective absorption gets in contact with the single-particle excitation continuum [45].

In addition to angle-resolved absorption, the intersubband response of the QW can also be probed in an edge-coupling geometry (see, e.g., Ref. [46]). The present formalism applies to edge coupling with a polished facet at a finite angle, as used in Ref. [19], by taking the electromagnetic field at the given incident angle in the substrate.

The transfer-matrix method can be applied to model an arbitrary number of QWs embedded in complex layered structures. The treatment is not limited to the long-wavelength approximation, as retardation effects can be included by calculating the coefficients $D_{\alpha,\alpha'}$ in Eq. (11). We notice that different but related formulations of the nonlocal theory have also been presented in the literature. In the long-wavelength approximation, the concept of sheet conductivity tensor can also be employed [34,47] and can be incorporated in a transfer-matrix formalism [36]. Moreover, this concept allows going beyond the random phase approximation and the linear response [48]. Another approach going beyond RPA has been formulated in Ref. [49]. It is also possible to model the response of a system of QWs in the long-wavelength approximation through an effective uniaxial dielectric tensor in the effective medium approximation, which has been extended to include nonlocal effects [36,50]. This approach works well even in the case of a small number of QWs [50], but it requires the additional constraint for the vertical length of the embedding structure (or the period, for periodic multiple-quantum-well systems) to be much smaller than the wavelength of light. Nevertheless, the effective medium approximation could prove itself useful when dealing with systems with a high density of QWs because it avoids performing algebraic calculations with a large number of transfer matrices.

---

[1]Notice that $\chi_{zz}^{(\mathrm{nl})}$ has the dimension of a length, as it is clear from Eqs. (19) and (21).

B. Long-wavelength approximation

In the $q \to 0$ and $k_z \to 0$ limits (neglecting nonparabolicity effects), all single-particle excitations are concentrated around the frequency ω_α and the single-particle susceptibility becomes

$$\chi_\alpha(\omega, q \to 0) = -\frac{\hbar e^2}{2\varepsilon_0 \omega_\alpha (m^*)^2} \frac{\Delta n_{2D,\alpha}}{(\omega + i\eta)^2 - \omega_\alpha^2}, \quad (15)$$

with $\Delta n_{2D,\alpha}$ the population density difference between subbands n and n'. In this case, it is possible to obtain a simple analytical expression for $\chi_{zz}^{(nl)}$. First, for each transition α we define the oscillator strength

$$f_\alpha = \frac{2m^* \omega_\alpha}{\hbar} z_\alpha^2 = \frac{\hbar}{2m^* \omega_\alpha} \left[\int dz\, \xi_\alpha(z) \right]^2 \quad (16)$$

(z_α is the intersubband dipole moment), the plasma frequency $\omega_{P,\alpha}$, and the effective length $L_{\text{eff},\alpha}$ (our definition is the same as in Ref. [13]):

$$\omega_{P,\alpha}^2 = \frac{e^2 \Delta n_{2D,\alpha}}{\varepsilon_0 \varepsilon_s m^* L_{\text{eff},\alpha}}, \quad (17)$$

$$L_{\text{eff},\alpha} = \frac{2m^* \omega_\alpha}{\hbar} \frac{1}{I_{\alpha,\alpha}}, \quad (18)$$

where the overlap integrals between intersubband currents are defined in Eq. (10). Following the derivation in Appendix A, we obtain that

$$\chi_{zz}^{(nl)}(\omega, \boldsymbol{q} \to 0) = -\sum_j \frac{\beta_j^2}{\omega^2 - \left(\Omega_j - i\frac{1}{2}\gamma_{nr,j} \right)^2}, \quad (19)$$

where Ω_j^2 are the eigenvalues of the coupling matrix

$$M_{\alpha,\alpha'} = \omega_\alpha^2 \delta_{\alpha,\alpha'} + \omega_{P,\alpha} \omega_{P,\alpha'} \frac{I_{\alpha,\alpha'}}{\sqrt{I_{\alpha,\alpha} I_{\alpha',\alpha'}}} \quad (20)$$

and the coefficients β_j are calculated from the corresponding normalized eigenvectors $\boldsymbol{\mathcal{E}}^{(j)}$ according to the relation

$$\beta_j = \sum_\alpha \omega_{P,\alpha} \mathcal{E}_\alpha^{(j)} \sqrt{f_\alpha L_{\text{eff},\alpha}}. \quad (21)$$

Notice that the coefficients are subjected to the Thomas-Reiche-Kuhn sum rule in the form

$$\sum_j \beta_j^2 = \frac{e^2 N}{\varepsilon_0 \varepsilon_s S m^*}, \quad (22)$$

where N is the total number of electrons that take part in intersubband transitions. Factor $\gamma_{nr,j}$ is a phenomenological rate accounting for the possible effect of incoherent scattering (i.e., homogeneous broadening of the optical transition due to a nonradiative decay channel).

The frequencies Ω_j are associated to a family of modes which can be called *multisubband plasmons*. In the long-wavelength limit, our semiclassical theory gives the same results for the frequencies Ω_j as the purely quantum mechanical theory developed in Ref. [13]. In particular, matrix (20) coincides with that obtained from the Hopfield-Bogoljubov transformation of the operators associated to bare intersubband transitions in the presence of electrostatic coupling. Physically, this means that the diagonal and off-diagonal coupling among

intersubband transitions induced by Coulomb interaction is fully taken into account by the nonlocal equation (6) with the proper boundary conditions. The coincidence of the semiclassical and quantum theories stems from the fact that the original Hamiltonian is quadratic in the photon and transition operators [33]. Yet, the semiclassical formulation can be used to derive a number of phenomenologically interesting quantities related to the optical properties, as we show in the next section.

III. RADIATIVE DECAY RATE

The transfer-matrix method offers a straightforward solution to problems involving electromagnetic radiation interacting with multisubband plasmons. In particular, for a generic transfer matrix $\mathbb{T}$, the reflection amplitude is given by the ratio

$$r = -\frac{T_{21}}{T_{22}}. \quad (23)$$

It is well known that the properties of both radiative and bound (polaritonic) states of the system can be calculated from the poles of the reflection coefficient [21], i.e., by the condition $T_{22} = 0$. Following Tait's classification [51], two different approaches can be employed. The *quasiparticle* solutions are obtained by setting a real in-plane wave vector and searching the poles in the complex-frequency plane. This corresponds to pure temporal damping [52] and such solutions have a direct physical interpretation in relation to luminescence or inelastic scattering experiments. On the other hand, the so-called *forced-harmonic* solutions are characterized by real frequencies and complex in-plane wave vectors. They have a direct interpretation in terms of optical spectra with monochromatic incident light. In this work, as we are interested in the problem of the radiative decay rate of multisubband plasmons, we will focus on quasiparticle solutions, for which the decay rate can be directly defined from the imaginary part of ω, according to the relation $\Gamma = -2\,\text{Im}\,\omega$.

In the simplest case, the transfer matrix is that of Eq. (12); this corresponds to the situation of a single QW embedded in an infinite medium with dielectric constant ε_s (equal to that of the barrier material), as illustrated by Fig. 2(a). According to Eq. (19), in the long-wavelength limit the condition $T_{22} = 0$
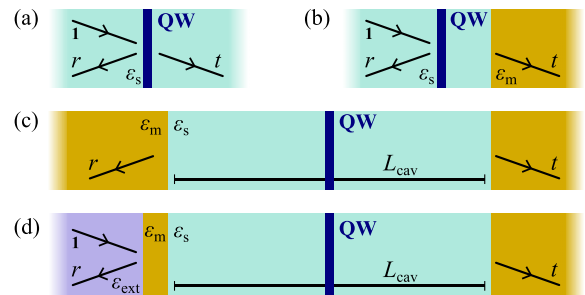

FIG. 2. (Color online) Some configurations for the QW considered in this work: (a) simple scattering problem; (b) scattering near a metallic mirror; (c) planar microcavity; (d) planar microcavity in the Kretschmann configuration. The corresponding transfer matrices are analyzed in the text.

becomes

$$1 + i\frac{q^2}{2k_z}\sum_j\left\{\beta_j^2 \bigg/ \left[\omega^2 - \left(\Omega_j - i\frac{1}{2}\gamma_{\mathrm{nr},j}\right)^2\right]\right\} = 0. \quad (24)$$

Following the perturbative approach, by looking for a solution in the form $\omega = \Omega_j - i\frac{1}{2}(\gamma_{\mathrm{nr},j} + \Gamma_{\mathrm{rad},j})$ at the first order in $\Gamma_{\mathrm{rad},j}$, we find that the radiative decay rate for multisubband plasmons has the expression

$$\Gamma_{\mathrm{rad},j}^{(\mathrm{pert})}(\boldsymbol{q}) = \frac{q^2}{2k_z\Omega_j}\beta_j^2 = \frac{q^2}{k_z k_{0,j}}\Gamma_{0,j}, \quad (25)$$

with

$$\Gamma_{0,j} = \frac{\sqrt{\varepsilon_s}}{2c}\beta_j^2, \quad (26)$$

$k_{0,j} = \sqrt{\varepsilon_s}\Omega_j/c$, and $k_z^2 = k_{0,j}^2 - q^2$. The perturbative decay rate is divergent for $q \to k_{0,j}$, as a result of a correspondent singularity in the photon density of states. The perturbative decay rate, however, represents only a low-q approximation. The actual decay rate can be calculated from the numerical solutions of Eq. (24), as shown in the following, at first for systems with a purely radiative decay dynamics ($\gamma_{\mathrm{nr},j} = 0$), and then including the presence of a finite incoherent scattering rate $\gamma_{\mathrm{nr},j}$.

A. Single intersubband plasmon

As a starting point for the discussion of radiative decay rates, we consider a system with a single IP, for instance a narrow QW with a single bright intersubband transition and for the moment we neglect the presence of nonradiative decay channels ($\gamma_{\mathrm{nr}} = 0$). The results that we present are consistent with those reported in Ref. [52] for an analogous system. Then, in the following section, we will extend our treatment to the case of multiple intersubband transitions.

The electromagnetic response of the QW with a single bright intersubband transition shows a resonance in the reflection coefficient at the IP frequency $\Omega_0 = (\omega_\alpha^2 + \omega_{P,\alpha}^2)^{1/2}$. The corresponding perturbative decay rate, according to Eq. (25), is

$$\Gamma_{\mathrm{rad}}(\boldsymbol{q}) = \frac{q^2}{k_z k_0}\Gamma_0 = \frac{\sin^2(\theta)}{\cos(\theta)}\Gamma_0, \quad (27)$$

with

$$\Gamma_0 = \frac{e^2 \Delta n_{2D} f_\alpha}{2m^*\varepsilon_0 c\sqrt{\varepsilon_s}} \quad (28)$$

and θ the angle of incidence of radiation, calculated from the normal to the QW. This result is in agreement with that calculated from the Fermi golden rule for a single intersubband plasmon [53], derived in Appendix B. Equations (27) and (28) are analogous to those of Z-polarized excitons in QWs [21].

A more complete picture of the decay rate is provided by the nonperturbative solutions of Eq. (24), which are shown by solid curves in Figs. 3(a) and 3(b), illustrating the frequency dispersion and the radiative decay rate $\Gamma_{\mathrm{rad}} = -2\,\mathrm{Im}\,\omega$, respectively. The latter is compared with the perturbative solution [dotted line in Fig. 3(b)]. As it is clear from Fig. 3(a), there are two separate branches in the dispersion of the modes: the radiative intersubband plasmon, whose dispersion starts
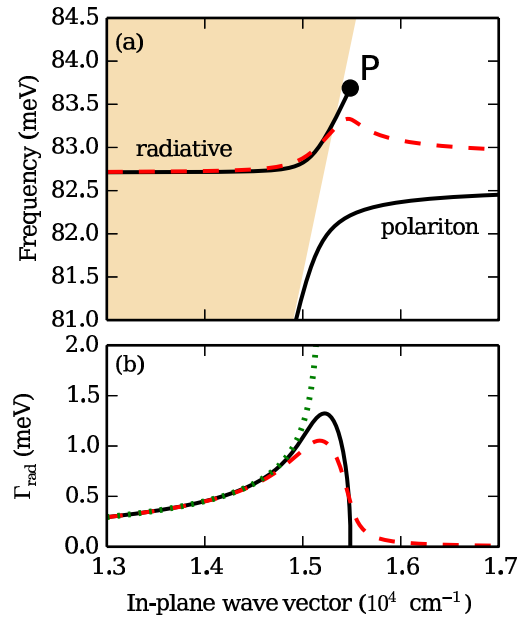

FIG. 3. (Color online) Solid curves: (a) dispersion of the radiative and polariton modes and (b) decay rate of the radiative mode, for the $1 \to 2$ intersubband plasmon of the same QW as in Fig. 1 ($n_{2D} = 1.5 \times 10^{12}$ cm^{-2}, $\gamma_{\mathrm{nr}} = 0$). Red dashed curves: (a) dispersion and (b) radiative decay rate for the case $\gamma_{\mathrm{nr}} = 1$ meV. Green dotted curve in (b): perturbative decay rate [Eq. (27)].

at $\omega = \Omega_0$ and ends at point P just outside the light cone, and a polariton mode (i.e., spatially confined along the z axis, similarly to the surface plasmon polariton at metal interfaces) in the region outside the light cone. The dispersion of the radiative mode is blue-shifted due to the interaction with light by an amount $\Delta = \mathrm{Re}\,\omega - \Omega_0 > 0$, in analogy with the Lamb shift of the hydrogen atom. The corresponding radiative decay rate follows closely the perturbative solution at low q, but it presents a broadening of the density-of-states singularity at $q = k_0$. The finite behavior of the decay rate around k_0 and the fact that the radiative branch ends slightly beyond the light cone can both be explained by the self-induced relaxation of energy conservation due to optical scattering of the IP itself.

The maxima of the nonperturbative decay rate and of the Lamb shift can be approximated in the single plasmon case by the expressions (valid for $\Gamma_0 \ll \Omega_0$)

$$\Gamma_{\mathrm{rad}}^{(\mathrm{max})} = \frac{\sqrt{3}}{2}\left(\Gamma_0^2\Omega_0\right)^{\frac{1}{3}}, \quad \Delta^{(\mathrm{max})} = \frac{1}{\sqrt[3]{4}}\left(\Gamma_0^2\Omega_0\right)^{\frac{1}{3}}, \quad (29)$$

which are formally identical to those reported in Ref. [22] for the case of a T-polarized QW exciton.[2] For the system in Fig. 3, with an electron density of 1.5×10^{12} cm^{-2}, we have a maximum decay rate of 1.3 meV, which corresponds to a lifetime $\tau = 1/\Gamma_{\mathrm{rad}} \simeq 500$ fs. Shorter life-times can be

---

[2]Electromagnetic modes for T-polarized QW excitons described in Ref. [22] follow a different equation with respect to intersubband plasmons, which are analogous to Z-polarized excitons, as we have already remarked. The two equations become coincident only in proximity of the light line ($k_z \simeq 0$).
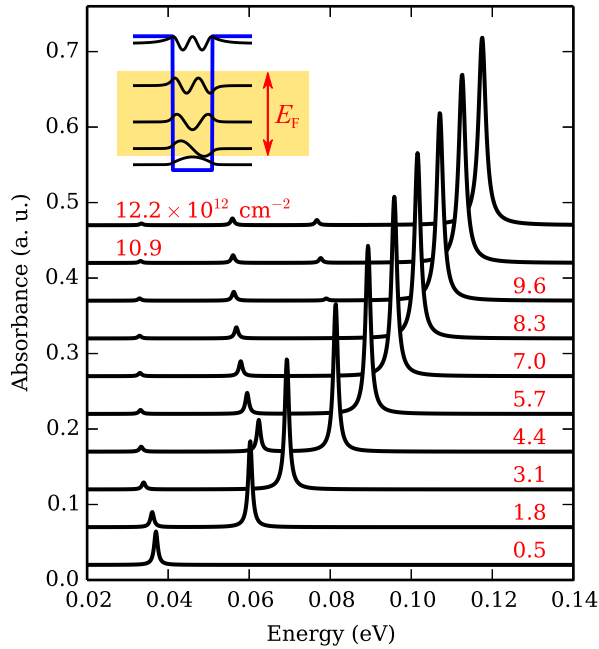
FIG. 4. (Color online) Absorbance of a 20-nm Al$_{0.3}$Ga$_{0.7}$As/
GaAs quantum well (see inset), as function of the frequency and
for several values of the two-dimensional electron density (indicated
by the labels in units of 10^{12} cm^{-2}), spanning the range in Fermi
energy indicated by the shaded area in the inset (zero temperature
and $\gamma_{\text{nr},j} = 1$ meV). Radiation is incident with a 45° angle from the
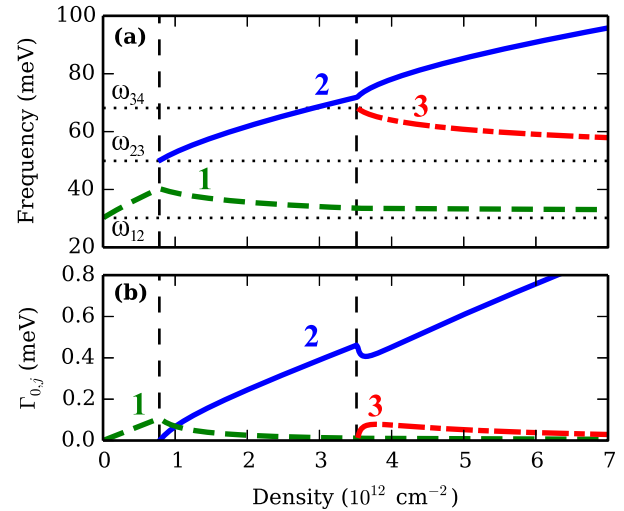normal.

FIG. 5. (Color online) (a) Frequencies and (b) perturbative decay
rates [more specifically, the $\Gamma_{0,j}$ terms in Eq. (26)] for three
multisubband plasmons ($j = 1,2,3$) of the same QW as in Fig. 4 as a
function of the electron density. The two vertical dashed lines indicate
where the second and third subbands start to populate, whereas the
horizontal dotted lines show the frequencies of bare intersubband
transitions (neglecting for simplicity the static Hartree correction,
which, however, is taken into account in the calculation of the plasmon
frequencies).

reached with electron densities above 10^{13} cm^{-2}, which can
be accomplished in particular QW structures [16]. Lifetimes
of the order of a few 100 fs have indeed been observed for
intersubband plasmons in QWs of 15–20 nm thickness [54].

Dashed curves in Fig. 3 show how the dispersion and
radiative decay rate of the radiative mode are modified in
the presence of a finite nonradiative rate $\gamma_{\text{nr}} > 0$. The most
evident feature is that the dispersion of the radiative mode
continues beyond point P; correspondingly, the radiative decay
rate presents a dissipation-induced tail at large in-plane wave
vector. The effects of nonradiative damping on the polaritonic
modes are nontrivial and they lead also to a modification of
the number of physically significant modes. For this reason,
we will treat them in more detail in a later section (Sec. III C).

B. Multiple intersubband transitions

In the presence of multiple intersubband transitions, e.g., in
the case of a large QW with a high doping level, the radiative
response of the system is modified with respect to the single-
transition behavior of the previous section. Figure 4 shows the
absorbance $A = 1 - |r|^2 - |t|^2$ of a 20-nm-thick QW with
varying two-dimensional electron density, calculated from
the transfer matrix in Eq. (12). As higher-energy subbands
become populated, new transitions become allowed and new
peaks appear in the electromagnetic response, reflecting the
increase of the number of IPs. However, the strength of
the absorption peaks is unequally distributed and it tends
to accumulate on a single bright multisubband plasmon. The
other multisubband plasmons tend to lose oscillator strength

and to become progressively dark as the doping level is
increased. The phenomenon originates from the electrostatic
interaction among the different intersubband transitions, which
is expressed in the $q \to 0$ limit by the coupling matrix in
Eq. (20)

The same behavior is illustrated in Fig. 5, which represents
the frequencies Ω_j and perturbative decay rates $\Gamma_{0,j}$ of three
selected multisubband plasmons ($j = 1,2,3$) as a function of
the doping density. The terms $\Gamma_{0,j}$ enter the expression for
the perturbative decay rate according to Eq. (25) and they are
directly proportional to the coefficients β_j^2 defined in Eq. (21).
The quantities Ω_j and $\Gamma_{0,j}$ plotted in Fig. 5 are directly related
to the positions and widths of peaks in Fig. 4, respectively. At
very low doping, there is a single IP associated to the $1 \to 2$
intersubband transition, whose decay rate is linear with the
doping density, in agreement with Eq. (28). When the second
subband starts to populate (as indicated by the vertical dashed
line around the density 0.8×10^{12} cm^{-2}), a new IP appears,
with the frequency ω_{23} associated to the $2 \to 3$ intersubband
transition. With the increasing of the density, its frequency
blue-shifts and its perturbative decay rate grows rapidly up
to including a large majority of the total available coupling
strength. Even when the third subband starts to populate (as
indicated by the second vertical dashed line), the new $j = 3$
intersubband plasmon, originating from the $3 \to 4$ transition,
rapidly loses most of its radiative strength in favor of the $j = 2$
plasmon. It is clear that these modes represent multisubband
plasmons that cannot be related to any particular transition any
more. In particular, the bright multisubband plasmon with $j =$
2 represents the cooperative response of the two-dimensional
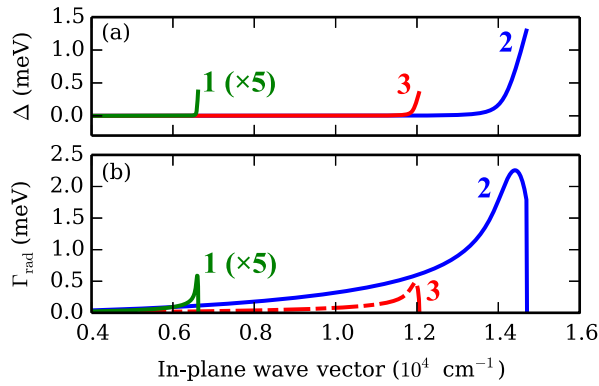electron gas, which dominates the optical response of the QW.

FIG. 6. (Color online) (a) Generalized Lamb shift and (b) non-perturbative decay rates of the three multisubband plasmons illustrated in Fig. 5, as a function of the in-plane wave vector. The electronic density of the QW is $4 \times 10^{12} \, \text{cm}^{-2}$. Data for the $j = 1$ plasmon have been multiplied by a factor 5 for visualization purposes.

These considerations are important to clarify the behavior of the Lamb shift and of the nonpertubative radiative decay rate as a function of the in-plane wave vector for different multi-subband plasmons, an example of which is shown in Fig. 6. The nonperturbative results, obtained by solving Eq. (24) in the complex-frequency plane, are displayed for the three previously discussed multisubband plasmons ($j = 1, 2, 3$) in the case of an electronic density $n_{2D} = 4 \times 10^{12} \, \text{cm}^{-2}$, corresponding to the Fermi level just above the minimum of the third subband. The dominance of the bright multisubband plasmon is already evident.

As a consequence, the radiative behavior of a QW with respect to the electron density could be classified into three different regimes. In the low-doping regime there is only a single populated subband and a weak radiative response following the description in Sec. III A. By increasing the doping, an intermediate regime is reached, characterized by a redistribution of the radiative strength among several multi-subband plasmons; eventually, the system is led to the bright multisubband plasmon regime, where the radiative behavior is dominated by a single plasmon similarly to Sec. III A, but with a far higher radiative decay rate, due to the in-phase response of multiple intersubband transitions (see Fig. 6). In view of the sum rule in Eq. (22), the perturbative decay rate of the bright multisubband plasmon can be still approximately described by Eq. (28), with $f_\alpha \simeq 1$. The coherent plasmon phenomenon has been strikingly demonstrated in a highly doped GaInAs/AlInAs QW with several occupied subbands [16].

C. Effect of nonradiative decay

In this section, we illustrate how the dispersion of radiative and polariton modes is modified by the presence of incoherent scattering, in the form of a nonradiative decay rate $\gamma_{\text{nr}, j} > 0$ in Eq. (24). Incoherent scattering has a strong influence on the electromagnetic response of the QW because not only does it modify the modal dispersion, but it also affects the total number of physically significant modes. This effect can be visualized more clearly in the complex-k_z plane. Modes with $\text{Im} \, k_z \geqslant 0$ represent polaritonic states spatially confined along the z axis,
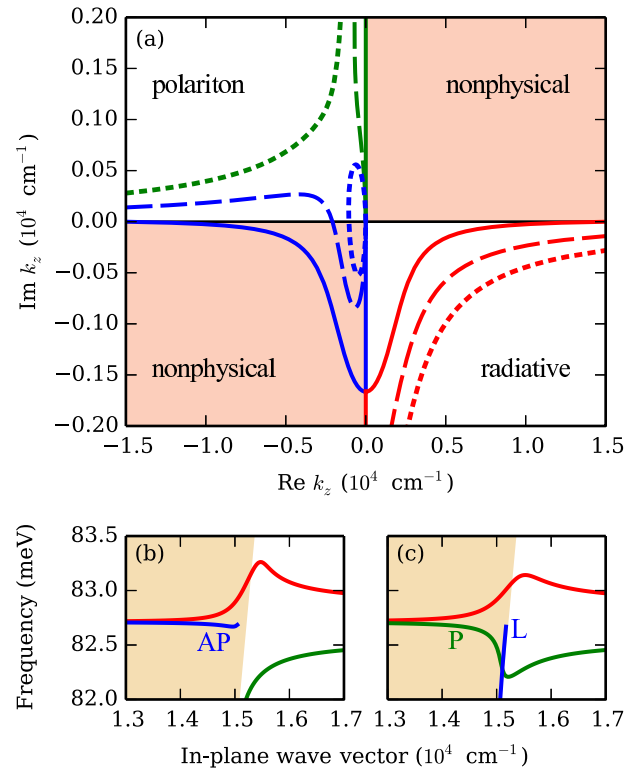

FIG. 7. (Color online) (a) The evolution of the poles of the reflection coefficient in the complex-k_z plane with varying the in-plane momentum, for different values of the nonradiative scattering rate γ_{nr}. Solid curves: $\gamma_{\text{nr}} = 0$; dashed curves: $\gamma_{\text{nr}} = 1.5 \, \text{meV}$ (both in the strong-coupling regime); dotted curves: $\gamma_{\text{nr}} = 3 \, \text{meV}$ (weak coupling). The system is the same as that in Fig. 3. (b), (c) The dispersion $\text{Re} \, \omega$ vs q in the cases (b) $\gamma_{\text{nr}} = 1.5 \, \text{meV}$ and (c) $\gamma_{\text{nr}} = 3 \, \text{meV}$ (nonphysical modes are excluded).

whereas modes with $\text{Im} \, k_z < 0$ represent radiative states [22]. In addition, assuming the temporal evolution $e^{-i\omega t}$ with $\text{Re} \, \omega \geqslant 0$, modes lying in the first ($\text{Re} \, k_z > 0$ and $\text{Im} \, k_z > 0$) and third ($\text{Re} \, k_z \leqslant 0$ and $\text{Im} \, k_z \leqslant 0$) quadrants of the complex plane are nonphysical since they present $\text{Im} \, \omega > 0$.

Here, we consider a system with a single intersubband plasmon, which, as we have seen, represents a good model of both a narrow low-doped QW with a single transition available and a thick heavily doped QW in the bright multisubband plasmon regime. Figure 7(a) shows the evolution of the poles of the reflection coefficient in the complex-k_z plane with varying the in-plane momentum q. Equation (24) for a single IP presents three distinct solutions (with the condition $\text{Re} \, \omega \geqslant 0$). For $\gamma_{\text{nr}} = 0$ they represent the radiative plasmon and the polariton modes, with the addition of a nonphysical mode with $\text{Im} \, \omega > 0$ in the third quadrant [solid curves in Fig. 7(a)]. With increasing the nonradiative rate γ_{nr}, the evolution of the poles in the complex-k_z plane is modified as shown by dashed curves in Fig. 7(a). The radiative mode in the fourth quadrant is downshifted, reflecting the formation of a dissipative tail at high q in the radiative decay rate, as we have already pointed out. Moreover, the nonphysical mode in the third quadrant is partially shifted to the second quadrant and it emerges as an "anomalous" polariton branch in the electromagnetic

dispersion [curve labeled "AP" in Fig. 7(b)]. This is an example of damping-induced dispersion branches, which are also found in the optical response of QW excitons [22].

Two distinct regimes are individuated. The threshold between the two regimes is given by the value γ_{th} of the nonradiative rate corresponding to the intersection between the dispersion of the anomalous damping-induced mode and the original polariton. In the limit $\Gamma_0 \ll \Omega_0$, the value can be approximated as

$$\gamma_{th} = \frac{3\sqrt{3}}{2\sqrt[3]{4}} \left(\Gamma_0^2 \Omega_0 \right)^{\frac{1}{3}},$$

i.e., it is of the same order of the maximum of the radiative decay rate. For instance, in the example of Fig. 7, the threshold is around $\gamma_{th} \simeq 2.5$ meV. When $\gamma_{nr} < \gamma_{th}$, in the underdamped or *strong-coupling* regime [dashed curves in Fig. 7(a) and graph (b)], the two polariton branches are well distinct. On the other hand, in the overdamped or *weak-coupling* regime [$\gamma_{nr} > \gamma_{th}$; dotted curves in (a) and graph (c)], polariton modes are merged in a continuous branch whose dispersion originates at Ω_0 and proceeds continuously to the high-q region [curve labeled "P" in Fig. 7(c)]. In addition, a distinct photonlike mode appears (curve labeled "L"), with a dispersion following closely the light line up to $\omega \simeq \Omega_0$. The situation is physically analog to the transition between the weak and strong coupling regimes in optical microcavities [55]; in particular, γ_{th} plays the role of the light-matter coupling parameter.

When dealing with experimental systems, it is particularly important to identify the regime of interest. In the strong-coupling regime, a clear signature of radiative effects is to be expected, in the form of a short radiative lifetime and strong Lamb shift in the resonance frequency. On the other hand, radiative effects become progressively less manifest in the weak-coupling regime, where the dynamics of the system is dominated by nonradiative relaxation. Notice that the anomalous polariton, in spite of lying inside the light cone, is a spatially confined state (Im $k_z > 0$), and thus it requires to be detected by means of near-field microscopy or similar methods.

IV. LAYERED SYSTEMS WITH METAL-DIELECTRIC INTERFACES

In most experiments, a thin layer of metal (usually gold) is laid on top of the QW structure to increase the amount of detected radiation. In other cases, the QW can be embedded in an optical cavity bound between two metallic mirrors to selectively couple intersubband transitions with a limited number of electromagnetic modes. In this section, we study these configurations in the context of the transfer-matrix approach.

A. Single metallic mirror

We consider the geometry sketched in Fig. 2(b), where the QW is separated by a spacer of length d and dielectric constant ε_s from a semi-infinite metallic mirror. The transfer matrix for the whole system is written as

$$\mathbb{T} = \frac{t_m}{1 - r_m^2} \begin{bmatrix} 1 & -r_m \\ -r_m & 1 \end{bmatrix} \mathbb{T}_d \, \mathbb{T}_{QW}, \qquad (30)$$

where r_m and t_m are the reflection and transmission amplitudes for the metal-dielectric interface, $\mathbb{T}_{QW}$ is the transfer matrix for the single QW in Eq. (12), and $\mathbb{T}_d = \text{diag}(e^{ik_z d}, e^{-ik_z d})$ is the propagation matrix for a slab of length d and dielectric constant ε_s. Radiative modes are still provided by the condition $T_{22} = 0$, which reads as in the $q \to 0$ limit

$$1 + i \frac{q^2}{2k_z} \sum_j \frac{(1 - r_m e^{ik_z(2d+L)}) \beta_j^2}{\omega^2 - \left(\Omega_j - i\frac{1}{2} \gamma_{nr,j} \right)^2} = 0. \qquad (31)$$

In particular, following the same procedure that led to Eq. (25), we obtain that the perturbative decay rate of multisubband plasmons is modified by the presence of the metallic interface in the form

$$\Gamma_{rad,j}^{(pert)}(q) = \left\{ 1 - \text{Re}\left[r_m e^{ik_z(2d+L)} \right] \right\} \frac{q^2 \, \Gamma_{0,j}}{k_z k_{0,j}}. \qquad (32)$$

This result is in agreement with electromagnetic calculations for the modification of the decay rate of a plane of radiating dipoles in proximity to a metallic surface and directed perpendicular to the surface. The decay rate of a single dipole can be obtained upon integration over in-plane wave vector q [56,57]. Moreover, such results are consistent with those reported in Ref. [52]. For an ideal (perfectly reflecting) metal with $r_m = -1$ and $k_z(2d + L) \ll 1$, we are left with the result that the perturbative decay rate in the presence of the mirror is *twice* the case of the isolated QW. For a real metal with dielectric function $\varepsilon_m(\omega)$, the reflection amplitude at the metal-dielectric interface reads as

$$r_m = \frac{\varepsilon_s \kappa - \varepsilon_m k_z}{\varepsilon_s \kappa + \varepsilon_m k_z}, \qquad (33)$$

with $\kappa^2 = \varepsilon_m(\omega) \omega^2/c^2 - q^2$. For noble metals, the difference in perturbative decay rate with respect to the ideal-metal behavior is small, except in close proximity to the light line ($q \simeq k_{0,j}$), when the singularity of the perturbative decay rate is cut off and the decay rate returns to zero. This discrepancy is not quantitatively significant because the perturbative approach fails in the $q \to k_{0,j}$ limit, but it is nonetheless a clear sign that the metal dispersion could have a strong effect on the QW radiative response for $q \simeq k_{0,j}$.

This fact is most evident from the nonperturbative decay rate of the intersubband plasmon, extracted from the numerical zeros of Eq. (31) and shown in Fig. 8 for the case of an ideal metal (solid curve), gold (dashed curve), and titanium (a metal with the very low plasma frequency $\omega_{pl} \simeq 2.5$ eV [58]; dashed-dotted curve). The decay rates correspond to short, sub-ps radiative lifetimes, down to $\sim$350 fs for the case of gold. Even in the case of gold, the maximum of the decay rate near k_0 is significantly modified in the real metal case with respect to the ideal one. The phenomenon could also be understood in terms of competition between the radiative decay channel and the surface plasmon polariton at the metal-dielectric interface, as it is suggested by the fact that, when the plasma frequency of the metal is closer to the IP frequency (e.g., in the case of titanium), the deviation with respect to the ideal case is more pronounced. Notice that the decay rate for real metals always presents a small dissipative tail at high q, similarly to the $\gamma_{nr} \neq 0$ case.
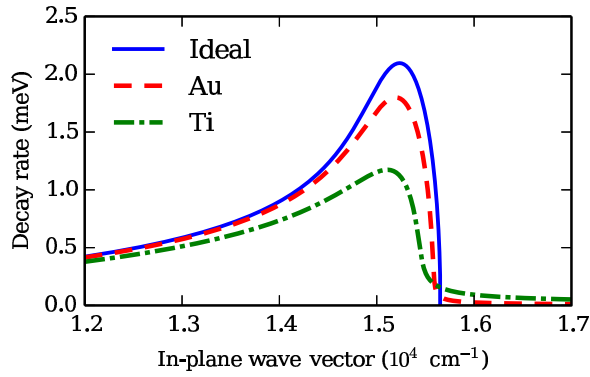
FIG. 8. (Color online) Decay rate for the same QW as in Fig. 3, when it is located in proximity to a metal-dielectric interface ($2d + L = 100$ nm), for ideal and real metals (Au and Ti). The dielectric function of real metals follows the Drude model with the parameters in Ref. [58].

To sum up, the present formulation allows calculating the change in radiative decay rate when the QW is placed in proximity to a metallic mirror. The behavior of the decay rate near the light line is very strongly dependent on the configuration of the system, including the dispersion of surrounding materials. Approximate formulas such as those presented in Eq. (29) could be useful for qualitative guidance, but a more detailed calculation taking into account the exact configuration of the system is in order to get quantitative results, as illustrated in this section. The transfer-matrix method allows us to generalize the procedure to more complex layered geometries.

B. Planar optical cavity

In order to increase radiation-matter interaction, a QW can be embedded in a dielectric slab bound between two metallic mirrors, so as to establish a planar optical cavity configuration. We suppose that the QW is located in the middle of a cavity of length $L_{\mathrm{cav}} = L_{\mathrm{QW}} + 2d$, bound by semi-infinite metallic mirrors, as shown in Fig. 2(c). The transfer matrix for such a system is derived in a straightforward manner from that of Eq. (30), in the form

$$\mathbb{T} = \frac{1}{1 - r_{\mathrm{m}}^2} \begin{bmatrix} 1 & -r_{\mathrm{m}} \\ -r_{\mathrm{m}} & 1 \end{bmatrix} \mathbb{T}_d \, \mathbb{T}_{\mathrm{QW}} \, \mathbb{T}_d \begin{bmatrix} 1 & r_{\mathrm{m}} \\ r_{\mathrm{m}} & 1 \end{bmatrix}.$$

The electromagnetic modes of the system are given by the condition $T_{22} = 0$, which reads as

$$r_{\mathrm{m}}^2 e^{ik_z L_{\mathrm{cav}}} - e^{-ik_z L_{\mathrm{cav}}}$$
$$+ iC\left[r_{\mathrm{m}}^2 e^{ik_z L_{\mathrm{cav}}} + e^{-ik_z L_{\mathrm{cav}}} - 2r_{\mathrm{m}}\right] = 0, \quad (34)$$

where the coefficient C, defined in Eq. (13), takes into account the nonlocal electrodynamic response of multisubband plasmons in the QW.

In the case of perfectly reflecting mirrors ($r_{\mathrm{m}} = -1$), Eq. (34) is simplified in the form

$$\sin(k_z L_{\mathrm{cav}}) + [1 + \cos(k_z L_{\mathrm{cav}})]C = 0. \quad (35)$$

Notice, in particular, that for $C = 0$ the expression reduces to the characteristic equation for TM modes of an ideal planar

cavity. As an example of application, if we suppose that the QW interacts with the TM_0 mode of the cavity, by expanding the equation at the first order in $k_z L_{\mathrm{cav}}$ and replacing Eqs. (13) and (19), we get

$$\varepsilon_{\mathrm{s}} \frac{\omega^2}{c^2} - q^2 \left[1 + \frac{1}{L_{\mathrm{cav}}} \sum_j \frac{\beta_j^2}{\omega^2 - \Omega_j^2} \right] = 0, \quad (36)$$

which represents an implicit equation for the dispersion of cavity polaritons.

We will briefly consider the case of a single intersubband plasmon, which has been extensively studied in the literature [13,35,36], and then we will move to the situation of a QW with multiple intersubband transitions. In the single IP case, Eq. (36) reads as

$$\varepsilon_{\mathrm{s}} \frac{\omega^2}{c^2} = \left(1 + \frac{L_{\mathrm{eff},\alpha}}{L_{\mathrm{cav}}} \frac{f_\alpha \omega_{P,\alpha}^2}{\omega^2 - \omega_\alpha^2 - \omega_{P,\alpha}^2} \right) q^2, \quad (37)$$

and its solutions are the well-known lower and upper cavity polariton branches, whose dispersion is characterized by an anticrossing behavior around the IP frequency. The minimal splitting between the branches, i.e., the Rabi splitting, is obtained as [13]

$$\Omega_{\mathrm{R}} = \frac{1}{2} \frac{\beta_j}{\sqrt{L_{\mathrm{cav}}}} = \frac{1}{2} \omega_{P,\alpha} \sqrt{\frac{f_\alpha L_{\mathrm{eff},\alpha}}{L_{\mathrm{cav}}}}. \quad (38)$$

With the increasing of the doping level inside the QW, a regime characterized by the presence of several multisubband plasmons is reached. In the single-cavity-mode approximation, the dispersion of intersubband polaritons is still provided by the solutions of Eq. (36); however, in this case, the interplay among different multisubband polaritons and collective effects such as those described in Sec. III B play a crucial role. By analogy with Eq. (38), one can define an effective Rabi frequency for each multisubband plasmon

$$\Omega_{\mathrm{R},j} = \frac{1}{2} \frac{\beta_j}{\sqrt{L_{\mathrm{cav}}}} \quad (39)$$

as a theoretical quantity providing an estimate of the coupling strength to the TM_0 cavity mode. The ratio $\Omega_{\mathrm{R},j}/\Omega_j$ between the Rabi and the resonance frequency is plotted in Fig. 9(a) as a function of the two-dimensional electronic density for the three multisubband plasmons of a 20-nm-thick QW already considered in Fig. 5. With increasing the density, at first the single IP regime, then a redistribution of the coupling strength among different multisubband plasmons, and, eventually, the emergence of the bright multisubband plasmon ($j = 2$) are clearly identified. Such results parallel for the case of cavity polaritons the analysis that we have carried out in Sec. III B for radiative decay rates.

The model in Eq. (36) does not take into account some important aspects, such as the presence of multiple electromagnetic cavity modes and the dispersive and dissipative response of the metallic plates. Moreover, from the experimental point of view, a coupling mechanism between cavity modes and external radiation is necessary. As a consequence, cavity modes acquire a finite broadening, which, together with the intrinsic nonradiative broadening of multisubband plasmons,
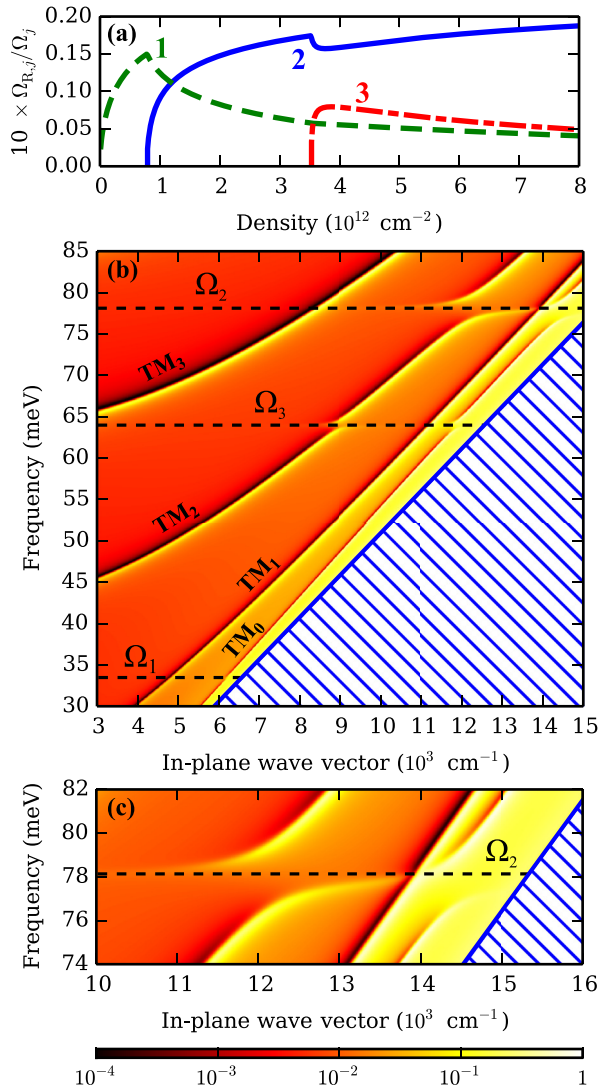
FIG. 9. (Color online) (a) The ratio $\Omega_{R,j}/\Omega_j$ [see Eq. (39)] for the same QW and the same three multisubband plasmons of Fig. 5. (b) Absorbance of the same QW ($n_{2D} = 4 \times 10^{12}$ cm^{-2}, $\gamma_{nr} = 0.5$ meV) placed in the center of 8-μm planar cavity bound by gold mirror in the Kretschmann configuration [see Fig. 2(d)]. Radiation impacts a 10-nm-thick gold mirror from a dieletric with $\varepsilon_{ext} = 15 > \varepsilon_s$. Dashed lines indicate the frequencies of the three multisubband plasmons of Fig. 5. The inaccessible region of the spectrum is indicated by the hatched region in the lower right corner of the plot. (c) Closeup of graph (b) around the frequency of the $j = 2$ multisubband plasmon.

affects the number of plasmons that can enter the strong-coupling regime of light-matter interaction. All these aspects can be readily addressed in the transfer-matrix formalism, by means of Eq. (34) and its generalizations to more elaborate structures. For instance, a more realistic metallic response can be taken into account by employing the metal-dielectric reflection coefficient in Eq. (33).

As an example, we consider an 8-μm-thick planar cavity bounded by gold mirrors in the Kretschmann configuration, sketched in Fig. 2(d). The left mirror is a 10-nm-thick film, in order to provide coupling with external radiation, and the QW is placed in the middle of the cavity. We consider the

same QW and multisubband plasmons discussed in Sec. III B and Fig. 9(a), with an electronic density of 4×10^{12} cm^{-2} (the Fermi level is just above the third subband). The absorbance $A = 1 - |r|^2 - |t|^2$ of the system is plotted in Fig. 9(b). Of the three multisubband plasmons in the frequency range under consideration, the $j = 1$ plasmon is in the weak-coupling regime and no anticrossing is visible in the dispersion. On the other hand, both the $j = 2$ and 3 plasmons are strongly coupled to the TM$_0$ and TM$_2$ cavity modes, despite the splitting of the $j = 3$ mode being far smaller (and barely recognizable in the TM$_0$ case). A closeup of the anticrossing behavior around the frequency of the $j = 2$ mode, i.e., the bright multisubband plasmon, is shown in Fig. 9(c). Notice that no anticrossing phenomena are formed in correspondence to odd TM modes of the cavity, as expected from symmetry consideration.

In our calculations, we neglected the *intrasubband* response of the QW. The intrasubband plasmon is in-plane polarized and, in the symmetric structure that we consider, it is decoupled from intersubband plasmons. In particular, the effect of the intrasubband response is to slightly modify the frequencies of the odd cavity modes, which do not interact with multisubband plasmons. Such modification can be expected to be weak since in our system the ratio L_{QW}/L_{cav} is small. We notice, however, that for systems including a large number of QWs, the effect of the intrasubband plasmon can be more significant and it can also affect the dispersion of intersubband cavity polaritons, as discussed in Ref. [36].

In summary, the dispersion characteristics of a particular mode can be engineered by tailoring the doping level and the position of the QW or the length of the cavity. The bright multisubband plasmon is particularly promising in view of reaching very high strengths of light-matter coupling. This has been experimentally confirmed in Ref. [16], which reports that the dispersion of the coherent multisubband cavity polariton has been verified for a stack of five 18.5-nm-thick QWs, showing a clear Rabi splitting $\hbar\Omega_R = 57$ meV. By applying the nonlocal semiclassical theory with the transfer-matrix formalism, it is possible to calculate the optical properties of intersubband plasmons in for QWs in complex arrangements with both dielectric and metallic layers. This opens the way towards more specific designs in view of achieving, e.g., stimulated scattering of multisubband plasmons.

V. CONCLUSIONS

We have presented a semiclassical theory of multisubband plasmons in semiconductor quantum wells. The collective optical response of the two-dimensional electron gas is strongly affected by Coulomb interaction among intersubband transitions, which is crucial in order to explain the formation of a coherent multisubband plasmon that takes up most of the coupling strength with radiation. These observed effects are fully captured by the present nonlocal formulation, which can be used for a full calculation of the optical properties of multisubband plasmons for QWs arranged in various geometries.

We have applied the theory to the study of the radiative decay rate of multisubband plasmons. Radiative lifetimes are short, of the order of a ps or below, and can be tailored by

means of the two-dimensional carrier density. The radiative decay rate calculated from perturbation theory is accurate far from the boundary of the light cone; however, in the opposite limit, the value of the decay rate is strongly dependent on the configuration of the system and a case-by-case calculation is generally in order, as we have shown in several examples, involving also the presence of metal-dielectric interfaces. In particular, in the case of a planar optical cavity, our formalism provides the dispersion of multisubband cavity polaritons. The presence of a nonradiative decay channel could play a major role in the relaxation dynamics of the QW, by triggering the appearance of damping-induced polaritonic modes.

We believe that the theory is presented in a sufficiently general manner for being applied in a straightforward way to more specific configurations of experimental interest, where it could prove itself useful both in the design and interpretation stages. An important research direction is to design structures that are suitable for the observation of quantum effects related to intersubband plasmons, like, e.g., stimulated scattering, in analogy to similar effects that have been demonstrated for QW exciton polaritons in microcavities [28,29]. In addition, the analysis reported in this work could help to clarify the dynamics of radiative relaxation by intersubband plasmons, which is gaining increasing interest both for fundamental physics studies and in view of practical applications in the field of mid- and far-infrared light emission.

APPENDIX A: LONG-WAVELENGTH LIMIT OF NONLOCAL THEORY

In this Appendix, we derive the $q \to 0$ and $k_z \to 0$ limits of the nonlocal susceptibility $\chi_{zz}^{(\mathrm{nl})}(\omega, \boldsymbol{q})$, which we have anticipated in Eq. (19). In this derivation, we neglect incoherent scattering ($\gamma_{\mathrm{nr},j} = 0$). In the long-wavelength limit, the linear problem in Eq. (9) reduces to the form

$$F_\alpha + \sum_{\alpha'} \frac{\chi_{\alpha'}(\omega, q \to 0) \, I_{\alpha, \alpha'}}{\varepsilon_\mathrm{s}} F_{\alpha'} = \int dz \, \xi_\alpha(z), \qquad \text{(A1)}$$

where we replace the $q \to 0$ expression for the single-particle susceptibility reported in Eq. (15). By defining the vectors $\tilde{\boldsymbol{F}}$ and $\boldsymbol{X}$, whose components are

$$\tilde{F}_\alpha = \frac{F_\alpha}{\omega^2 - \omega_\alpha^2} \frac{\omega_{P,\alpha}}{\sqrt{I_{\alpha,\alpha}}}, \quad X_\alpha = \frac{\omega_{P,\alpha}}{\sqrt{I_{\alpha,\alpha}}} \int dz \, \xi_\alpha(z),$$

Eq. (A1) becomes $(\omega^2 - \mathbb{M}) \tilde{\boldsymbol{F}} = \boldsymbol{X}$, with the coupling matrix $\mathbb{M}$ presented in Eq. (20).

By solving the eigenproblem for the matrix $\mathbb{M}$ and writing it in the form $\mathbb{M} = \mathbb{U} \boldsymbol{\Omega}^2 \mathbb{U}^{-1}$, where $\boldsymbol{\Omega}^2$ is the diagonal matrix of the eigenvalues Ω_j^2 and $\mathbb{U}$ is the orthogonal matrix of the column eigenvectors, the solution of the linear problem is straightforward:

$$\tilde{\boldsymbol{F}} = \mathbb{U} \frac{1}{\omega^2 - \boldsymbol{\Omega}^2} \mathbb{U}^{-1} \boldsymbol{X}.$$

In the same $q \to 0$ limit, the nonlocal susceptibility in Eq. (14) can be written $\chi^{(\mathrm{nl})} = -\boldsymbol{X}^T \tilde{\boldsymbol{F}}$, from which we obtain

$$\chi^{(\mathrm{nl})} = -[\mathbb{U}^{-1} \boldsymbol{X}]^T \frac{1}{\omega^2 - \boldsymbol{\Omega}^2} \mathbb{U}^{-1} \boldsymbol{X}. \qquad \text{(A2)}$$

The result in Eq. (19) derives directly from the observation that $\mathbb{U}^{-1} \boldsymbol{X}$ is just the vector of the β_j's [see also Eq. (16)].

APPENDIX B: PERTURBATIVE DECAY RATE FOR INTERSUBBAND PLASMONS

In the following, the radiative decay for a system with a single intersubband plasmon is calculated from the Fermi golden rule in quantum theory. The quantum operator $b_{\boldsymbol{q}}^\dagger$ associated to the bright $1 \to 2$ intersubband transition in a QW reads as

$$b_{\boldsymbol{q}}^\dagger = \frac{1}{\sqrt{\Delta N}} \sum_\sigma \sum_{k_{F2} \leqslant k \leqslant k_{F1}} c_{2,\boldsymbol{k}+\boldsymbol{q},\sigma}^\dagger c_{1,\boldsymbol{k},\sigma}, \qquad \text{(B1)}$$

where $c_{n,\boldsymbol{k},\sigma}^\dagger$ is the creation operation for the state in subband n with in-plane momentum $\boldsymbol{k}$ and spin σ. The sum is over all states involved in the transition; in particular, $\sum_\sigma \sum_k = \Delta N$ and $\Delta n_{2\mathrm{D}} = \Delta N / S$, with S the area of the sample. As an effect of electrostatic interaction in the two-dimensional electron gas, resonance frequency is shifted from the frequency of the bare transition ω_{12} to the frequency of the intersubband plasmon $\Omega_0 = (\omega_{12}^2 + \omega_{P,12}^2)^{1/2}$. The operator associated to the IP is obtained through a Hopfield-Bogoljubov transformation of the original transition operator [13]

$$p_{\boldsymbol{q}}^\dagger = \frac{\Omega_0 + \omega_{12}}{2\sqrt{\omega_{12} \Omega_0}} b_{\boldsymbol{q}}^\dagger + \frac{\Omega_0 - \omega_{12}}{2\sqrt{\omega_{12} \Omega_0}} b_{-\boldsymbol{q}}; \qquad \text{(B2)}$$

correspondingly, the wave function of an excited plasmon is $|\boldsymbol{q}_\mathrm{pl}\rangle = p_{\boldsymbol{q}}^\dagger |0\rangle$ ($|0\rangle$ being the transformed vacuum).

Radiation-matter interaction is described by the Hamiltonian $H_\mathrm{I} = -\boldsymbol{d} \cdot \boldsymbol{E} = -ez E_z$, with the electric field operator

$$\boldsymbol{E}(\boldsymbol{r}) = i \sum_{\lambda,\boldsymbol{k}} \left(\frac{\hbar c k}{2\varepsilon_0 \varepsilon_\mathrm{s} V} \right)^{\frac{1}{2}} \boldsymbol{\mathcal{E}}_{\boldsymbol{k},\lambda} [a_{\boldsymbol{k},\lambda} e^{i\boldsymbol{k}\cdot\boldsymbol{r}} + \mathrm{H.c.}].$$

Then, the matrix element between a photon with wave vector $\boldsymbol{k}$ and a plasmon with in-plane momentum $\boldsymbol{q}$ reads as

$$\langle \boldsymbol{k}_\mathrm{ph} | H_\mathrm{I} | \boldsymbol{q}_\mathrm{pl} \rangle = -iez_{12} \left(\frac{\Delta N \hbar \omega_{12} c k}{2\Omega_0 \varepsilon_0 \varepsilon_\mathrm{s} V} \right)^{\frac{1}{2}} \boldsymbol{\mathcal{E}}_{\boldsymbol{k},\lambda} \cdot \hat{\boldsymbol{z}} \, \delta_{\boldsymbol{k}_\parallel, \boldsymbol{q}},$$

where $\boldsymbol{k}_\parallel$ is the in-plane component of $\boldsymbol{k}$ and z_{12} is the intersubband dipole momentum. Only the TM electric field has a non-null z component and interacts with the intersubband transition. In particular, we easily calculate that $\sum_\lambda |\boldsymbol{\mathcal{E}}_{\boldsymbol{k},\lambda} \cdot \hat{\boldsymbol{z}}|^2 = k_\parallel^2 / k^2$. Finally, from the Fermi golden rule, we obtain

$$\Gamma_{\boldsymbol{q}} = \frac{2\pi}{\hbar} \sum_\lambda \sum_{\boldsymbol{k}} |\langle \boldsymbol{k}_\mathrm{ph} | H_\mathrm{I} | \boldsymbol{q}_\mathrm{pl} \rangle|^2 \, \delta(\hbar\Omega_0 - \hbar c k)$$

$$= \frac{q^2}{k_0 k_z} \Gamma_0 = \frac{\sin^2(\theta)}{\cos(\theta)} \Gamma_0, \qquad \text{(B3)}$$

with

$$\Gamma_0 = \frac{e^2 \Delta n_{2D}}{\hbar \varepsilon_0 c \sqrt{\varepsilon_s}} z_{12}^2 \omega_{12} \qquad (B4)$$

($k_0 = \sqrt{\varepsilon_s} \Omega_0 / c$ and $k_z^2 = k_0^2 - q^2$). Equation (B3) presents the same result as Eq. (27), as it can be seen by comparison with Eq. (16). The same result is reported also in Ref. [53]. Notice

that, by using the bare intersubband operator $b_q^\dagger$ instead of the plasmon operator $p_q^\dagger$, i.e., by putting $\Omega_0 = \omega_{12}$ everywhere, the depolarization shift in the resonance frequency is lost, but the value of Γ_0 in Eqs. (28) and (B4) remains unaltered. This is related to the fact that the term Γ_0 gives an estimate of the coupling strength with the external field, independently of the microscopic dynamics of the two-dimensional electron gas.

[1] S. Allen, D. Tsui, and B. Vinter, Solid State Commun. **20**, 425 (1976).
[2] W. Chen, Y. Chen, and E. Burstein, Surf. Sci. **58**, 263 (1976).
[3] T. Ando, Solid State Commun. **21**, 133 (1977).
[4] M. Nakayama, Solid State Commun. **21**, 587 (1977).
[5] D. A. Dahl and L. J. Sham, Phys. Rev. B **16**, 651 (1977).
[6] B. Vinter, Phys. Rev. B **15**, 3947 (1977).
[7] T. Ando, A. B. Fowler, and F. Stern, Rev. Mod. Phys. **54**, 437 (1982).
[8] M. Helm, in *Intersubband Transitions in Quantum Wells: Physics and Device Applications I*, Semiconductors and Semimetals, Vol. 62, edited by H. C. Liu and F. Capasso (Academic, San Diego, CA, 1999), Chap. 1, p. 1.
[9] M. Załużny, Phys. Status Solidi B **123**, K57 (1984).
[10] M. Załużny, Physica B+C (Amsterdam) **128**, 171 (1985).
[11] S. K. Chun, D. S. Pan, and K. L. Wang, Phys. Rev. B **47**, 15638 (1993).
[12] L. Wendler and E. Kändler, Phys. Status Solidi B **177**, 9 (1993).
[13] Y. Todorov and C. Sirtori, Phys. Rev. B **85**, 045304 (2012).
[14] A. Pinczuk, H. Störmer, R. Dingle, J. Worlock, W. Wiegmann, and A. Gossard, Solid State Commun. **32**, 1001 (1979).
[15] A. Pinczuk, G. Abstreiter, R. Trommer, and M. Cardona, Solid State Commun. **30**, 429 (1979).
[16] A. Delteil, A. Vasanelli, Y. Todorov, C. Feuillet Palma, M. Renaudat St-Jean, G. Beaudoin, I. Sagnes, and C. Sirtori, Phys. Rev. Lett. **109**, 246808 (2012).
[17] B. Askenazi, A. Vasanelli, A. Delteil, Y. Todorov, L. C. Andreani, G. Beaudoin, I. Sagnes, and C. Sirtori, New J. Phys. **16**, 043029 (2014).
[18] C. Ciuti, G. Bastard, and I. Carusotto, Phys. Rev. B **72**, 115303 (2005).
[19] A. Delteil, A. Vasanelli, Y. Todorov, B. Paulillo, G. Biasiol, L. Sorba, and C. Sirtori, Appl. Phys. Lett. **102**, 031102 (2013).
[20] K. Cho, J. Phys. Soc. Jpn. **55**, 4113 (1986).
[21] F. Tassone, F. Bassani, and L. Andreani, Il Nuovo Cimento D **12**, 1673 (1990).
[22] C. Creatore and A. L. Ivanov, Phys. Rev. B **77**, 075324 (2008).
[23] V. M. Agranovich and O. A. Dubovskii, Pis'ma Zh. Eksp. Teor. Fiz. **3**, 345 (1966) [JETP Lett. **3**, 223 (1966)].
[24] E. Hanamura, Phys. Rev. B **38**, 1228 (1988).
[25] L. C. Andreani, F. Tassone, and F. Bassani, Solid State Commun. **77**, 641 (1991).
[26] B. Deveaud, F. Clérot, N. Roy, K. Satzke, B. Sermage, and D. S. Katzer, Phys. Rev. Lett. **67**, 2355 (1991).
[27] For a review on nonlocal electrodynamics and radiative lifetime of two-dimensional excitons, see also L. C. Andreani, in *Strong Light-Matter Coupling: From Atoms to Solid-State Systems*, edited by A. Auffèves, D. Gerace, M. Richard, S. Portolan,

M. França Santos, L. C. Kwek, and C. Miniatura (World Scientific, Singapore, 2014), Chap. 2, p. 37.
[28] P. G. Savvidis, J. J. Baumberg, R. M. Stevenson, M. S. Skolnick, D. M. Whittaker, and J. S. Roberts, Phys. Rev. Lett. **84**, 1547 (2000).
[29] J. Kasprzak, M. Richard, S. Kundermann, A. Baas, P. Jeambrun, J. M. J. Keeling, F. M. Marchetti, M. H. Szymańska, R. André, J. L. Staehli, V. Savona, P. B. Littlewood, B. Deveaud, and L. S. Dang, Nature (London) **443**, 409 (2006).
[30] A. Yariv and P. Yeh, *Optical Waves in Crystals* (Wiley, New York, 1984).
[31] L. C. Andreani, Phys. Lett. A **192**, 99 (1994).
[32] G. Panzarini, L. C. Andreani, A. Armitage, D. Baxter, M. S. Skolnick, V. N. Astratov, J. S. Roberts, A. V. Kavokin, M. R. Vladimirova, and M. A. Kaliteevski, Phys. Rev. B **59**, 5082 (1999).
[33] G. Panzarini, L. C. Andreani, A. Armitage, D. Baxter, M. S. Skolnick, V. N. Astratov, J. S. Roberts, A. V. Kavokin, M. R. Vladimirova, and M. A. Kaliteevski, Phys. Solid State **41**, 1223 (1999).
[34] V. G. Avramenko, J. Opt. Soc. Am. B **23**, 1872 (2006).
[35] A. Liu, Phys. Rev. B **55**, 7101 (1997).
[36] M. Załużny and W. Zietkowski, Phys. Rev. B **88**, 195408 (2013).
[37] P. J. Feibelman, Phys. Rev. B **12**, 1319 (1975).
[38] A. Bagchi, Phys. Rev. B **15**, 3060 (1977).
[39] A. Eguiluz and A. Maradudin, Ann. Phys. (NY) **113**, 29 (1978).
[40] P. Harrison, *Quantum Wells, Wires and Dots*, 2nd ed. (Wiley, New York, 2005).
[41] Equation (3) holds in the approximation that in the light-coupling Hamiltonian we neglect the small difference in the effective mass between the well and barrier materials and its eventual energy dependence due to nonparabolicity.
[42] U. Ekenberg, Phys. Rev. B **40**, 7714 (1989).
[43] M. Załużny, Phys. Rev. B **43**, 4511 (1991).
[44] M. Załużny, Solid State Commun. **82**, 565 (1992).
[45] R. J. Warburton, K. Weilhammer, J. P. Kotthaus, M. Thomas, and H. Kroemer, Phys. Rev. Lett. **80**, 2185 (1998).
[46] J. B. Williams, M. S. Sherwin, K. D. Maranowski, and A. C. Gossard, Phys. Rev. Lett. **87**, 037401 (2001).
[47] O. Keller, J. Opt. Soc. Am. B **12**, 987 (1995).
[48] I. Waldmüller, Ph.D. thesis, Technische Universität Berlin, 2004.
[49] V. Despoja, M. Šunjić, and L. Marušić, Phys. Rev. B **80**, 075410 (2009).
[50] M. Załużny and C. Nalewajko, Phys. Rev. B **59**, 13043 (1999).
[51] W. Tait, Phys. Rev. B **5**, 648 (1972).
[52] L. Wendler and T. Kraft, Phys. Rev. B **60**, 16603 (1999).
[53] C. Ciuti and I. Carusotto, Phys. Rev. A **74**, 033811 (2006), Eq. (74). Notice that the result differs by a factor 2 because

the rate is defined from the half width at half maximum of the resonance.

[54] T. Laurent, Y. Todorov, A. Vasanelli, A. Delteil, I. Sagnes, G. Beaudoin, and C. Sirtori (unpublished).

[55] L. C. Andreani, G. Panzarini, and J.-M. Gérard, Phys. Rev. B **60**, 13276 (1999).

[56] R. R. Chance, A. Prock, and R. Silbey, in *Advances in Chemical Physics*, Vol. 37, edited by I. Prigogine and S. A. Rice (John Wiley & Sons, Hoboken, NJ, 1978), Chap. 1, p. 1.

[57] G. Ford and W. Weber, Phys. Rep. **113**, 195 (1984).

[58] M. A. Ordal, R. J. Bell, J. R. W. Alexander, L. L. Long, and M. R. Querry, Appl. Opt. **24**, 4493 (1985).